Crystallinity, Supermolecular Structure, and Thermodynamic Properties of Linear Polyethylene Fractions

J. Maxfield and L. Mandelkern*

Department of Chemistry and Institute of Molecular Biophysics, Florida State University, Tallahassee, Florida 32306. *Received June 9, 1977*

ABSTRACT: The supermolecular structures or morphologies of crystallized molecular weight fractions of linear polyethylene, covering the range $M = 2.53 \times 10^4$ to 8.0×10^6, were studied by small-angle light scattering complemented by polarized light microscopy. The different forms that can be developed were established as a function of molecular weight and crystallization temperatures. The best defined, or most perfectly developed spherulites, are formed after rapid crystallization (quenching) for $M \leq 8.5 \times 10^5$. This organized structure deteriorates as the molecular weight is increased under these crystallization conditions. The range $M = 1\text{–}2 \times 10^6$ represents a transitional region where the scattering pattern is very sensitive to molecular weight distribution and details of the quenching process. For higher molecular weights, however, an azimuthally independent light-scattering pattern is observed which can be attributed to randomly oriented crystalline lamella. The lowest molecular weight samples yield thin rod-like structures at all isothermal crystallization temperatures. For intermediate molecular weights, as the crystallization temperature is raised, there is a transition from poorly defined spherulites to rods whose lengths are comparable to their breadth. At the higher molecular weights, randomly oriented crystallites are found at all crystallization temperatures. It is possible to develop samples having the same degree of crystallinity, on a density basis, but which have quite different supermolecular structures. These differences are reflected in other thermodynamic quantities, such as the enthalpy of fusion, which are not only dependent on the degree of crystallinity but on the morphology as well. The possible influence of the supermolecular structure (at the same level of crystallinity) on physical and mechanical properties is portended by these results. Possible mechanistic explanations for the formation of the different morphological forms, which are still in a rudimentary state of development, are briefly discussed.

It has been established that virtually all properties of bulk crystallized polymers are extremely dependent on the molecular weight and crystallization temperature.[1–3] An extremely wide range in properties can be achieved by utilizing molecular weight fractions and varying the crystallization temperature (or undercooling) under which crystallization takes place. These properties correlate well with the levels of crystallinity and the molecular structure of the lamella crystallites and the associated interfacial and amorphous regions.[1–3] The further organization of the lamellar crystallites into higher levels of morphology, or supermolecular structure, are well known. Until recently, a spherulitic morphology was thought to be the universal mode of homopolymer crystallization, although other forms such as ovoids and hedrites had been noted for specific polymers.[4–6] These were thought to be special or restricted cases.

Since there is this very large effect of molecular weight and crystallization temperature on properties, it is obviously important to ascertain whether they are accompanied by any changes in the supermolecular structure. In the first study of this type, utilizing molecular weight fractions of linear polyethylene, four different morphological forms could be identified from their small-angle light-scattering patterns.[7] These were subsequently confirmed by polarized light microscopy.[8] This first study,[7] which was designed to test the concept of different morphological forms with molecular weight, was essentially restricted to rapid crystallization processes and was thus exploratory in nature. However, for this mode of crystallization the results are valid. For rapid crystallization, spherulitic structures were observed in all samples with $M = 9 \times 10^5$ or less. For the higher molecular weights within this range the spherulites formed showed a high degree of imperfection. In the range $M = 1\text{–}2 \times 10^6$ rodlike aggregates of lamellae were observed. At still higher molecular weights, $M = 3\text{–}8 \times 10^6$, although the levels of crystallinity are of the order of 50%, no specific morphology is observed and the pattern is interpreted as coming from the random orientation of lamellae crystallites. Thus under these crystallization conditions, at least, the supermolecular structure is strongly dependent on molecular weight.

The influence of polydispersity has also been explored in binary mixtures.[8] The addition of a high molecular weight fraction (nonspherulitic forming) to a spherulite forming one causes a progressive deterioration in the morphology. The addition of a relatively small amount causes a major decrease in the spherulite size and further addition causes the complete loss of structure. However, mixing two fractions, each of which in the pure state yields spherulites, has no effect on the resulting morphology. An extreme sensitivity to small changes in molecular weight distribution is indicated by these results, particularly when different forms are involved in the components of the distribution. Caution will have to be exercised when interpreting results and when comparing different fractions and the results of different investigations. It has also been noted that spherulitic structures can be induced in the very high molecular weight fractions when they are crystallized from a highly swollen diluent mixture.[8] These latter results, although preliminary in nature, must have a direct bearing on the mechanism of spherulite formation.

The fact that different morphological forms can be easily developed with rapid crystallization makes for an obvious inquiry under isothermal crystallization conditions for as high a temperature or as low an undercooling as possible. Working with fractions is, of course, mandatory. Studies of the overall crystallization rate of linear polyethylene have shown that by using fractions the range of isothermal crystallization can be significantly extended.[9] Thus, at this point in the investigation of the problem not only are fractions necessary for any definitive study, for reasons indicated above, but the previous work has shown[9] that a more extensive temperature range can be encompassed by their use. Since a larger temperature range was studied for the overall rate of crystallization, a much better analysis could be made of the temperature coefficient of the process.[9] The conventional plot, where the rate is plotted against the nucleation temperature function, is no longer linear except for the higher molecular weights. The slopes in these plots for the high molecular weights and the high temperature lower molecular weights are essentially the same. They are about twice as great as the low temperature (isothermal) low molecular weight slope.[9] These conclusions

Table I
Characterization of Linear Polyethylene Fractions

Sample source	$M_n \times 10^{-3}$	$M_\eta \times 10^{-3}$	$M_w \times 10^{-3}$	M_w/M_n
SNPA	25.3		27.8	1.10
SNPA	42.0		46.2	1.10
SNPA	72.8		80.8	1.11
SNPA	145.0		161.0	1.11
SNPA	217.2		252.0	1.16
HIFAX 28		418		
HIFAX 16		850		
HIFAX 16		1500		
HIFAX 16		2490		
HIFAX 28		3000		
HIFAX 16		4000		
HIFAX 16		6000		
HIFAX 28		8000		

are not dependent on the type of nucleation process assumed. The results strongly suggest a change in crystallization mechanisms with temperature, for $M \lesssim 1 \times 10^6$, and a similarity between the high temperature lower molecular weights and the high molecular weights at all temperatures.

In a preliminary isothermal crystallization study[8] for $M = 6.6 \times 10^5$ it was found that spherulites were formed at the lower crystallization temperatures. However, for crystallization above about 127 °C the morphology was nondistinct. These observations were made by small angle light scattering and confirmed by direct light microscopy. These results thus give support to the qualitative ideas suggested above. However, the temperature at which the change in morphology occurs is several degrees lower than the change in slope in the overall crystallization rate study.

In a more extensive study, using light microscopy as the observational technique, Hoffman et al.[10] studied the growth rate of spherulites and axialites of polyethylene fractions over the accessible range of isothermal crystallization temperatures. Molecular weights over the range 3×10^3 to 8×10^5 were studied. As will be discussed in more detail subsequently, several different morphological forms were identified depending on the molecular weight and crystallization temperature. It is interesting to note at this point that the change from an axialite to spherulite morphology takes place at a rather well-defined temperature. This change is characterized by a factor of 2 difference in the temperature coefficient of the growth rate. There is, therefore, a close similarity to the changes previously reported[9] in the overall rate of crystallization and with it the strong suggestion that they both have the same origin.

In this present work we have extended our previous studies in much more detail with respect to isothermal crystallization over the accessible temperature range including long-time crystallization at low undercoolings. A major addition to all previous experimental work has been the extension of the molecular weight range studied, for fractions, by an order of magnitude to 8×10^6. Small angle light scattering (SALS) was the major experimental technique used here. This method offers some major advantages over light microscopy in studying the supermolecular structure. The subjectiveness of the interpretation of the morphological types because of the possible confined field of view is eliminated as are any anomalies caused by the need of very thin films in light microscopy. The radii of spherulites are easily determined from the SALS patterns and the complication of overlapping spherulites is avoided. However, since certain nonspherulitic morphological forms yield very similar SALS patterns (see below) the interpretation can be ambiguous. In these cases light microscopy can discriminate between them and thus serves as a convenient adjunct to the major technique.

The major objective of this work was to ascertain the different morphological forms that could be found in linear polyethylene and to establish the molecular weight and crystallization temperature for their formation. We are also interested in the different properties exhibited by the diverse supermolecular structures. In the present work we concentrate on the relationship between the thermodynamic quantities that have been found. Although this study is not directly or specifically concerned with the kinetics and mechanism of the development and growth of the specific morphological forms certain general criteria that will need to be fulfilled will become clear. Thus, because of the larger molecular weight range studied certain ground rules are established which will set the basis for future development.

Experimental Section

The polyethylene fractions used in this work were either produced in this laboratory by fractionation of Hifax 16 and Hifax 28 or were obtained from S.N.P.A.. The Hifax polymers are linear polyethylenes obtained from Hercules Powder Co. The viscosity average molecular weight of Hifax 16 is 2×10^6. Hifax 28 has a viscosity average molecular weight of 7×10^6 and a number average molecular weight of 2×10^5. The Hifax fractions were produced by liquid–liquid separation methods previously described[11] and the molecular weight obtained from the intrinsic viscosity using the equation given by Chiang.[12] The fractions obtained from Societe Nationale des Petroles D'Aquitaine (S.N.P.A.) were prepared by gel permeation chromatography. All the fractions used in this work, as well as the molecular weight data, are listed in Table I.

All the samples were prepared by the same method. A thin film was first made by melting the sample in vacuo at 165 °C between the plates of a Carver press. The pressure used was between 5 000 and 15 000 lb/in.^{2} for the lowest and highest molecular weights, respectively. After melting, the sample was quickly removed from the press and plunged into a dry ice/2-propanol mixture. This method produces thin films of ca. 50 μm which have the lowest attainable levels of crystallinity for each molecular weight. A portion of each sample was retained for SALS and polarized light microscopy studies.

The remainder of these rapidly crystallized films were used to prepare the high temperature isothermally crystallized samples. Small portions of the film were wrapped in aluminum foil and sealed under vacuum in glass tubes. These samples were then melted for 2 h in an oil bath at 155 °C and then quickly transferred to the crystallization bath at the required temperature. The samples were kept at each crystallization temperature for times which were well in excess of the time necessary to complete isothermal crystallization. The required times to accomplish this were determined from the dilatometric studies of the overall rate of crystallization.[9] At the completion of the isothermal crystallization the samples were slowly cooled to room temperature. The measurements were made under these conditions.

The SALS and polarized light microscopy techniques were used to study both the rapidly quenched and isothermally crystallized films. The SALS studies were carried out with an instrument similar to that described by Stein and co-workers.[13] The degree of crystallinity was obtained from density measurements in an 2-propanol–water gradient column at 23 °C, using the specific volume relations of Chiang and Flory.[14] The enthalpy of fusion was determined in the conventional manner previously described.[15,16]

Results and Discussion

Theoretical and Light-Scattering Background. It has already been noted in earlier preliminary work that several distinctly different SALS patterns, and variants thereof, are observed in linear polyethylene depending on molecular weight and crystallization temperature.[7,8] To interpret the results reported in the present work it is helpful, and almost mandatory, to examine in detail the theoretical basis for the different scattering patterns. The variety of patterns that can be observed, and their interpretation, is a major advantage of this method over direct light microscopic studies. However, we shall find that light microscopy studies are a very useful adjunct to the SALS.

The type patterns obtained from spherulitic structures have been widely observed. The theoretical basis have been cal-

culated by Stein and others.[17] The H_v scattering obtained can be described by the relation

$$I_{H_v} = C_3 V^2 \left\{ \frac{3}{U^3} (\alpha_t - \alpha_r) \cos^2 \left(\frac{\theta}{2}\right) \sin \mu \cos \mu \times (4 \sin U - U \cos U - 3(\mathrm{Si})U \right\}^2 \quad (1)$$

where V is the volume of the spherulite, U is the reduced angle $((4\pi R/\lambda) \sin (\theta/2))$, R is the radius of the spherulite, μ is the azimulthal scattering angle, α_r and α_t are the parallel and perpendicular components of the polarizability and

$$(\mathrm{Si})U = \int_0^U \left(\frac{\sin X}{X}\right) dX$$

The pattern in this case is clearly fourfold symmetric based on the $\sin \mu \cos \mu$ dependence. Maxima occur at $\mu = (\pi/4) + (n\pi/2)$. Although not immediately apparent from the intensity relation, it can easily be shown that there is also an intensity maxima in θ (at $\mu = 45$) given by

$$U_{max} = 4\pi(R/\lambda) \sin (\theta/2) = 4.1 \quad (2)$$

The resulting pattern from this type of scattering has the characteristic four-leaf clover appearance. This pattern has been observed in a variety of polymer systems[18–22] including linear polyethylene under special conditions.[7,8] Its observation in the present work will be discussed below in further detail.

A variant of this theoretical pattern is observed where there is scattering present for $\mu = 45°$ at low angles. This type of scattering has been described as "tennis racquet" shaped and can be explained theoretically in terms of multiple scattering and imperfections within the spherulites[23–26] and has been observed in linear polyethylene.[8] A further degeneration of the spherulite pattern can also be observed. Although there is still a fourfold symmetry there is no longer a well-defined maximum in θ at $\mu = 45°$. Thus, there are three different types of spherulitic patterns, which can be distinguished from one another. They essentially represent different levels of order within the spherulite. For convenience we shall designate these as types (a), (b), and (c), respectively, in the subsequent discussion.

SALS patterns are also observed which are nonspherulitic.[27,28] Most of the theoretical models that have been suggested and calculated for these situations arise from the scattering of rods. We shall not present at this time a complete survey of all the different theories that have been proposed.[28–35] Rather, we shall restrict ourselves to a discussion of two models which can be considered to be representative of the general theoretical arguments and which also provide a more than adequate basis for the interpretation of our results.

The first of these models was developed by Kawai[36] and assumes a random assembly of anisotropic rods whose optical axis is inclined at an angle ω_0 with respect to the rod direction and is fixed in a plane defined by an azimuthal angle δ. this model describes an anistropic body such as a fibrillar arrangement of lamellar structures. Only the length of the rod is of consequence in this model. We shall designate this as model A because of the fixed angle δ. The equations for the H_v scattered intensity are more complex than for spherulites. The basic functional form satisfies for present purposes. We can write:[36]

$$I_{H_v} = K_1 \{[\alpha(\theta) \sin^2 \mu \cos^2 \mu + \beta(\theta)] P_4(\cos \omega_0) A(U) + \delta(\theta) P_2 (\cos \omega_0) B(U) + C(U)\} \quad (3)$$

where K_1 is a constant; $\alpha(\theta) = 420 \cos^2 (\theta/2)$; $\beta(\theta) = 12 - 60 \cos^2 (\theta/2)$; $\gamma(\theta) = 60 \cos^2 (\theta/2) - 40$; $A(U) = (1/U^5)([U^3/6] - [(2U^2 - 1)/8] \sin 2U - (U/4) \cos 2U)$; $B(U) = (1/2U^2)(1 - [\sin 2U/2U])$; $C(U) = 28 [(\sin 2U/U)([1 - \cos 2U]/2U^2)]$; and $U = (2\pi L/\lambda) \sin (\theta/2)$. This equation is also fourfold symmetric in μ. However, the type of scattering is now dependent on $P_4(\cos \omega_0)$, which is the fourth order Legendre function in ω_0. For $P_4 > 0$, or $\omega_0 < 30°30'$ and $\omega_0 > 70°07'$, the scattering pattern is of the X type, i.e., the pattern describes the figure X and we shall classify it as a type (d) pattern. This type pattern has essentially the same characteristics as that classified earlier as type (c). This is reasonable since the patterns arise from similar basic structures, i.e., anisotropic aggregates of crystallites. However, as will be seen below, these two patterns arise from two quite different morphologies when observed using polarized light microscopy. This method is used to distinguish between the two when they occur.

For $P_4 = 0$, or $\omega_0 = 30°33'$ and $70°07'$, the pattern is circularly symmetric and is designated type (f). For $P_4 < 0$, or $30°33' < \omega_0 < 70°07'$, the pattern is of the + type, i.e., it describes the figure + and is designated as (e). Thus three different scattering patterns can be obtained for this model. The pattern observed is critically dependent on ω_0, the angle between the optical axis and the long axis of the rod. Experimentally, this would correspond to the angle between the chain axis and the longer lateral axis of the fibrils. The length of the rods can be estimated for the H_v intensity by comparing the intensity at $\mu = 0$ and 45° as a function of θ, i.e., $(I_{H_{v\mu=45°}} - I_{H_{v\mu=0}})$ is a maximum for θ given by

$$4.8 = (2\pi L/\lambda) \sin (\theta_{max}/2) \quad (4)$$

where L is the length of the rod.

In a generalization of this rodlike model, designated here as B, the angle θ is allowed to vary randomly.[37] The optical element is still inclined at an angle θ, but only circular symmetry of the element about the rod axis is maintained. Such a model would be applicable when the rods or fibrils are twisted around their fibrillar axes with a twisting period which is irregular and short compared to the wavelength of the illumination. This model would be compatible with nonringed spherulites or any system of irregular fibrils. The H_v scattering in this case has the following functional form:

$$I_{H_v} = K_2 [P_2(\cos \omega_0)]^2 [\delta_1(\theta) \sin^2 \mu \cos^2 \mu + \beta_1(\theta)] \quad (5)$$

where K_2 is a constant; $\delta_1(\theta) = A(U) \cos^4 (\theta/2)$; $\beta_1(\theta) = 1/7 [(8B(U) - A(U)) \cos^2 (\theta/2) + 1/15(3A(U) - 80B(U) + 56C(U))]$; and $A(U)$, $B(U)$, and $C(U)$ are defined previously. This relation is again fourfold symmetric in μ. However, there is no P_4 dependence, and hence the angle ω_0 only affects the absolute intensity, and not the shape of the pattern which is again an X type for all ω_0 and is the type (d) in our classification scheme. This result is in sharp contrast to the more restricted model, A, where there are three different H_v patterns to be expected depending on the value of ω_0. The length of the rod is given by the same relation as in the previous case.

Both of these models contain the primary assumption that the rods have an infinitesimal width. Calculations have also been made which allow the rods in both models to have a finite width.[35] In this case the fourfold symmetry becomes less well defined as the width of the rod is increased. The pattern becomes circularly symmetric as the width becomes comparable to the length. We shall designate it as (g) since it represents a quite different scattering structure, although the pattern is similar to (f).

The scattering pattern for randomly arranged lamellae can be deduced by considering the results for model A.[56] For the sake of convenience, we can consider random lamellae as being equivalent to a rod in which the optical axis is allowed to vary randomly, i.e.,

$$\langle P_2(\cos \omega_0) \rangle = \langle P_4(\cos \omega_0) \rangle = 0 \quad (6)$$

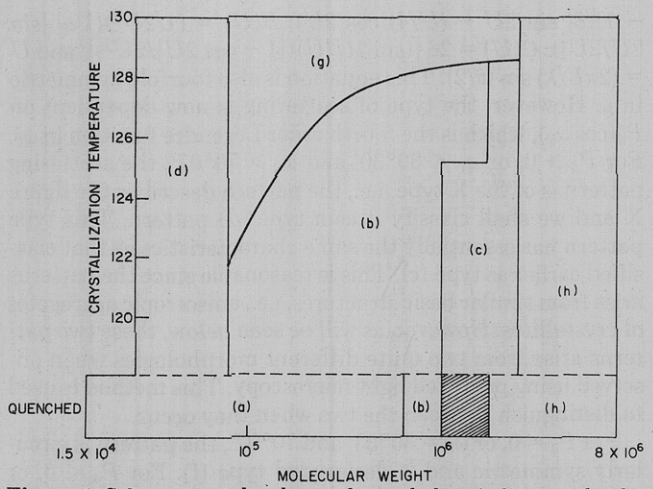

Figure 1. Schematic of the observed morphology in linear polyethylene fractions as a function of molecular weight and crystallization conditions. The letters in parentheses refer to the types of morphology described in the text.

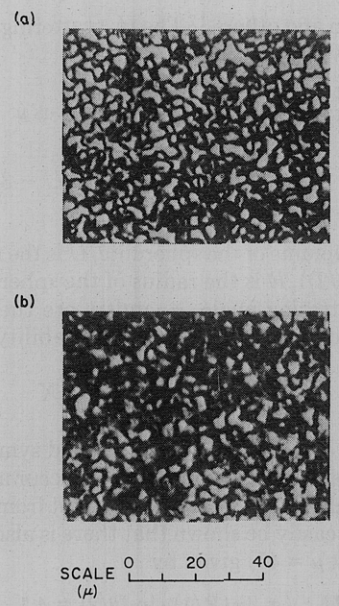

Figure 2. Polarized light micrographs from rapidly crystallized (quenched) fractions: (a) $M_w = 2.78 \times 10^4$; (b) $M_\eta = 8.5 \times 10^5$.

In this situation the scattering is circularly symmetric. We shall designate its patterns as (h). This pattern can appear similar to the rod patterns (g) and (f) in that all three are circularly symmetric in scattering angle θ. The random structures giving rise to the (h) pattern are easily distinguished, however, from the two rod structures by polarized light microscopy. Hence this method is used to clarify the morphology when a circularly symmetric SALS pattern is observed.

It should be noted at this point that these models only represent several among many. They have been selected to help give an insight into the experimental results obtained here. The most important assumption in these models is that the scattering is calculated for a single isolated rod. A more general approach would be to use the method of Prud'homme and Stein[34] for a correlated assembly of anisotropic rods. However, this model is conceptually more complicated to interpret and in any event gives calculated intensity patterns which follow the broad trends of the simpler isolated rod models.

With this background of scattering theory we can now present our experimental results. We interpret them in terms of the supermolecular structure formed.

Experimental Results

Rapidly Crystallized (Quenched) Films. The SALS data for quenched samples are in general agreement with the results reported by Go et al.[7] We shall, therefore, only briefly discuss these results concentrating on any differences from the previous report and on the additional thermodynamic data that we have obtained in the present work.

For molecular weight from 1.54×10^4 to 8.5×10^5 spherulitic SALS patterns are observed which are very similar to those previously reported.[7] When observed through a polarized microscope with crossed polars, these samples all show the Maltese cross extinction patterns characteristic of spherulites. The sample 8.5×10^5 shows considerable extra scattering at small angles in the SALS patterns which has been called a "tennis-racket" pattern.[17] The SALS results for these molecular weights can be divided into two groups according to the classification scheme described above. Molecular weights 1.5×10^4 to 4.18×10^5 are of type (a) or ordered well-developed spherulites. Molecular weight 8.5×10^5 is of type (b) or "tennis racket" scattering.

We, thus, duly record these two results in Figure 1. This figure will eventually represent a complete schematic diagram of the dependence of the morphological and supermolecular structures formed on molecular weight and crystallization temperature. We can note, in advance of a complete discussion of the diagram, that type (a), well-developed spherulites, are only formed within a restricted but fairly large molecular weight range under very rapid crystallization conditions. The sizes of the spherulites observed here are typically ~5 μm radius. This is only fractionally smaller than that reported previously.[7] This difference is not particularly significant and can be most probably attributed to the slightly lower crystallinities obtained here. This subject will be discussed below in more detail.

When observed through a polarizing microscope, with crossed polars, these samples all show the Maltese cross extinction patterns characteristic of spherulites. In agreement with the SALS the polarized light micrographs for these molecular weights also indicate that the spherulites are less ordered at the higher molecular weights than at the lower molecular weights. This is illustrated in Figure 2 where we show light micrographs for molecular weight 2.78×10^4 and 8.5×10^5.

For molecular weights $1–2 \times 10^6$ azimuthally dependent patterns have been reported[7] under these crystallization conditions. They have been attributed to aggregates of lamellae approximately 1–10 μm in size with some degree of preferred orientation. In the present work we observe an azimuthally independent pattern for $M = 1.56 \times 10^6$ as is shown in Figure 3a. For $M = 1.89 \times 10^6$ a spherulitic pattern of type (b) is observed as in Figure 3b. The morphology in this molecular weight range is clearly transitional and is apparently very sensitive to molecular weight or molecular weight distribution, as well as the details of the quenching procedure and film thickness. The morphology associated with the azimuthally independent pattern is discussed below with the results for the higher molecular weights. This transitional molecular weight range is indicated by the cross-hatched area in Figure 1.

For molecular weights from 2.49×10^6 to 8×10^6 an azimuthally independent pattern is also observed. This pattern, which is type (h) in our classification scheme, was also previously reported[7] for these molecular weights and attributed to randomly oriented lamellae. Typical light micrographs and SALS patterns for this molecular weight range, similar to those found here, have already been reported. The SALS

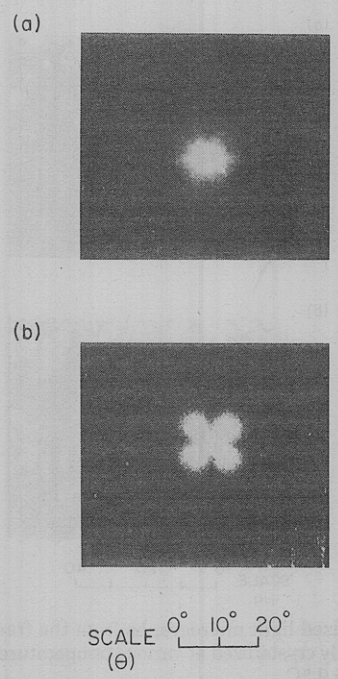

Figure 3. H_v small-angle light-scattering patterns from rapidly crystallized (quenched) fractions with molecular weights in the region 1–2 × 10^6: (a) $M_\eta = 1.5 \times 10^6$; (b) $M_\eta = 1.89 \times 10^6$.

patterns by themselves are only indicative of scattering from small, of the order of the wavelength of the incident light, randomly oriented scattering elements which do not give any information on the microscopic arrangements of the crystallites. Previous electron microscopy studies of the debris remaining after selective oxidation with fuming nitric acid have indicated the presence of lamellae for quenched as well as for isothermally crystallized samples.[38] Thus the randomly oriented crystallites, located in the region marked (h) in Figure 1, are most probably arranged in lamellae, but with less organization between them than is observed at lower molecular weights.

Further evidence that the crystallite organization is different in this high molecular weight region comes from the density and enthalpy of fusion associated with these samples. Density and enthalpy of fusion determinations of the level of crystallinity for all the quenched samples are shown in Table II. The degree of crystallinity calculated from the density shows that, except for the very lowest molecular weight, there is virtually no change in crystallinity with molecular weight. These results are in good agreement with previous reports.[15] The crystallinity determined from enthalpy is in fairly good agreement with that from density up to $M_w = 8.5 \times 10^5$. For higher molecular weights there is a considerable decrease in the value calculated from the enthalpy. These results are illustrated more clearly in Figure 4 which is a plot of the difference in the levels of crystallinity obtained by the two methods against the molecular weight. There is a very distinct discontinuity in the curve at a molecular weight of approximately 10^6. This molecular weight corresponds almost exactly to the region where the transition from spherulitic to nonspherulitic morphology occurs, with a loss in the organized crystallite structure. These results will also be examined subsequently in conjunction with the thermodynamic data obtained for the other crystallization temperatures studied.

Discrepancies in the degree of crystallinity calculated by both methods have been reported previously[15] but have not been heretofore identified with specific differences in the morphological form or supermolecular structure. On the most general grounds a reduced value for the measured enthalpy

Table II
Degree of Crystallinity of Quenched Samples

Molecular wt × 10^{-3}	Level of crystallinity (quenched)	
	Density	Enthalpy of fusion
27.8	0.64	0.68
80.8	0.55	0.48
161		0.56
252	0.50	0.44
418	0.55	
850	0.53	0.49
1500	0.57	0.35
2490	0.53	0.34
6090	0.55	0.30

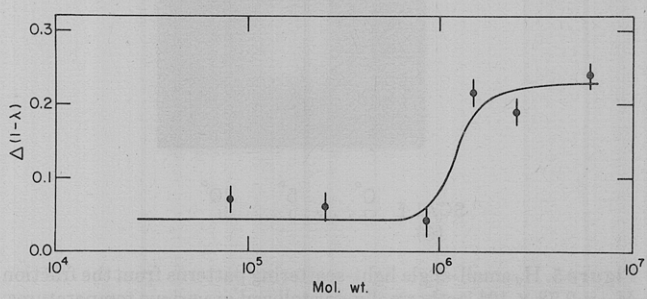

Figure 4. Plot of the difference in level of crystallinity (1 − λ) as measured by density and enthalpy of fusion as a function of molecular weight for rapidly crystallized (quenched) fractions.

of fusion can be attributed to several factors.[15] They are either an increase in the concentration of defects within the interior of the crystallites or to a decreased crystallite thickness or increased interfacial enthalpy. The latter possibility would reflect a change in the molecular structure of the crystallite surface or a complete change in crystallite form. Obviously, just the determination of the enthalpy of fusion cannot distinguish between the possibilities.

The SALS scattering patterns for the quenched whole unfractionated polymers were also studied. The results generally agree with those given above. The lower molecular weight Marlex-50 yields very good spherulites. They are larger than those observed with the fractions and show a definite ring structure under the polarized microscope. This result indicates that for this polymer the spherulites are highly organized. Thus Marlex-50 gives the same result as for a fraction of the same weight average molecular weight with, however, a greater degree of order within the spherulites. This result can probably be attributed to the presence of significant amounts of very low molecular weight material known to be present in this polymer. As has been alluded to previously[8] there is a rather strong influence of polydispersity on the resulting morphology. This aspect of the subject is going to have to be studied in much more systematic detail before any conclusions regarding broadly distributed systems can be made.

The two Hi-Fax samples show different scattering patterns. Hi-Fax-16 ($M_\eta = 2 \times 10^6$) gives a predominatly azimuthally independent pattern. There is, however, a very weak fourfold symmetry superimposed upon it. The highest molecular weight sample ($M_n = 2 \times 10^5$, $M_\eta = 7 \times 10^6$) only yields patterns which are attributable to random scattering elements. In this case the viscosity average corresponds to a fraction yielding random scattering elements, but the number average molecular weight corresponds to the formation of well-developed spherulites (type a). The results with the Hi-Fax samples, based on viscosity average molecular weights, are consistent with the transition region illustrated in Figure 1.

It has been established that adding a small amount of a high

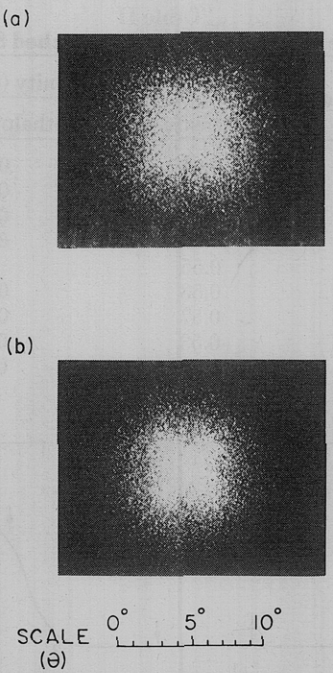

Figure 5. H_v small-angle light-scattering patterns from the fraction $M_w = 2.78 \times 10^4$ isothermally crystallized at various temperatures: (a) $T_c = 130.0$ °C; (b) $T_c = 125.9$ °C.

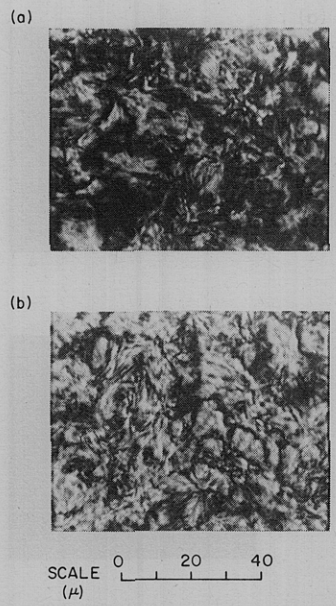

Figure 6. Polarized light micrographs from the fraction $M_w = 2.78 \times 10^4$ isothermally crystallized at various temperatures: (a) $T_c = 130.0$ °C; (b) $T_c = 125.9$ °C.

molecular weight nonspherulite forming fraction to a spherulite forming one has a dominant effect on the morphology. It first causes a reduction in size and then disappearance of the spherulites when only a relatively small amount is added. For more complex molecular weight distributions, or for the three unfractionated samples, the results are not as yet predictable. Thus, the major emphasis in this work is given to the fractions and only the results for this type of sample are summarized in Figure 1.

Isothermally Crystallized Samples. The results obtained for the fractions can be conveniently divided into three groups: (i) $M_w < 4.62 \times 10^4$; (ii) $M_w = 8.08 \times 10^4$ to $M_\eta = 2.49 \times 10^6$; (iii) $M_\eta = 3.0 \times 10^6$ to $M_\eta = 8.0 \times 10^6$. One sample with $M_\eta = 4 \times 10^6$ falls into group (ii) instead of group (iii). In the quenched situation just described this sample yields random scattering elements. This is the only molecular weight anomaly that we have found for the isothermal crystallizations. In the first group, two samples were studied, 2.78×10^4 and 4.62×10^4. Crystallization was carried out in the isothermal region (125–130 °C) as described previously. Typical SALS and light microscopy results on these films are shown in Figures 5 and 6. The SALS shows a fourfold symmetric H_v pattern of type (d) for the range of observation indicated in Figure 1. Interpretations of this pattern in terms of the theoretical models previously discussed indicate a morphology where there is a correlation in orientation of the lamellae or groups of lamellae. An exact calculation of the size of the scattering elements requires a quantitative investigation of the dependence of the intensity on azimuthal angle. However, one can obtain a rough estimate of the size from the intensity of the patterns at $\mu = 0$ and 45°. The size thus calculated from eq 4 is the order of 10 μm. The light microscopy data show the presence of rodlike structures of approximately 10–20 μm in length. In order to determine the direction of the birefringence of these structures the following observations were made. It has long been known that spherulites of polyethylene are negatively birefringent.[39] Thus if a quarter-wave plate is inserted between the polarizer and the objective and the polarizer and analyzer are crossed, quadrants of the spherulite parallel to the quarter-wave plate will appear dark and those perpendicular bright. If this experiment is done on the rodlike structures shown in Figure 6 the same effect is observed indicating that these structures grow with their lamellae oriented in the same manner as spherulites. Hence it is established that there is no special mode of crystal growth occurring here. The SALS data for the sample $M_w = 4.62 \times 10^4$ shows a less well pronounced fourfold symmetry. This probably is mostly due to a decrease in the length to width ratio of the rods as discussed in the theoretical section. The light microscopy data are indistinguishable from those for $M_w = 2.78 \times 10^4$. A sample of $M_w = 2.78 \times 10^4$ was also prepared by allowing the film to cool slowly directly from the melt. The results were identical with those shown in Figures 5 and 6. This observation establishes the important point that spherulites in linear polyethylene are only developed in this molecular weight range when the sample is cooled rapidly from the melt.

The H_v scattering pattern in this range, as is illustrated in Figure 5, is of the X type and thus can be described by either Model B or by Model A with $\omega_0 = 0 \rightarrow 30°33'$ or $\omega = 70°07' \rightarrow 90°$. The size of the rods determined from the experimental data is ~20 μm irrespective of the model chosen. This dimension corresponds very closely with those for the structures seen in the polarized light micrographs of Figure 6. The H_v scattering data cannot distinguish between Models A or B. However, the V_v scattering pattern for these samples is of the + type with the largest scattering lobe at $\mu = 0°$. This scattering pattern is consistent with that calculated for Model A with $\omega_0 = 70°$.[37] Furthermore it has been suggested[40–42] that the *b* crystal axis is oriented radially in a spherulite, while the *a* and *c* axes are tangential. If the same basic growth mechanism applies to the rodlike morphology observed here then Model A would be favored. This is supportive of a value of ω_0 between 70 and 90°, since the possibility of the alignment being between 0 and 30° can be eliminated because of the birefringence. Finally, Raman scattering from polyethylene has shown that the *c* axis can be oriented at an angle of up to 60° from that of the growth direction of the lamella.[43] This result is consistent with the interpretation presented here. The observed pattern is not strongly fourfold symmetric as would be expected for ideal isolated rods of infinitesimal thickness. However, better agreement with the theoretical models can be obtained if we allow the rods to have a finite thickness. Comparison of the data with theoretically predicted intensi-

Table III
Levels of Crystallinity Obtained from Density and Enthalpy of Fusion Measurements for Isothermally Crystallized Fractions[a]

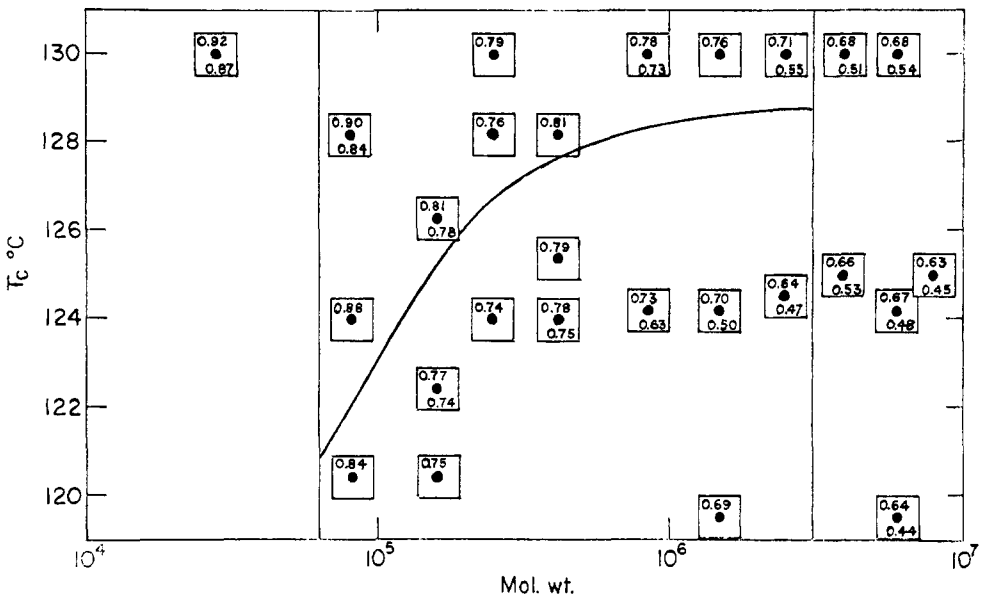

[a] The exact molecular weight and crystallization temperature for each set of measurements is denoted by •, the crystallinities by, i.e.,

$$\frac{(1-\lambda)_d}{(1-\lambda)_{\Delta H}}$$

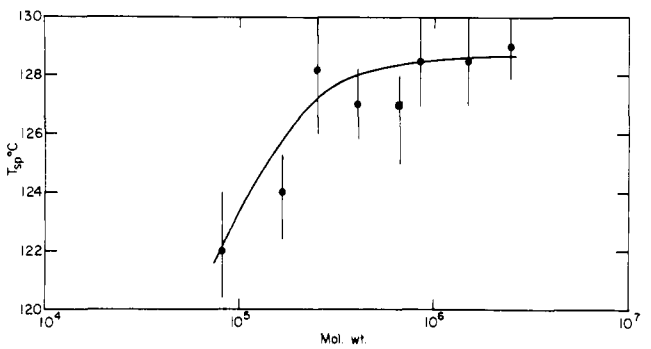

Figure 7. Plot of the temperature (T_{sp}) where a change is observed in the morphology of isothermally crystallized fractions as a function of molecular weight: (●) our data, (■) from ref 11.

ties for rods of finite thickness[35] suggests that the structures have a width to length ratio of approximately 0.2. These dimensions correspond to structures about 2–4 μm wide which agree with the light micrographs.

In summary the SALS data obtained from the samples in this group have been analyzed in general terms of rods or rod aggregates of type (d) as illustrated in the schematic of Figure 1 with length approximately ~20 μm and width about 4 μm. The data strongly suggest that the *a* and *b* axes are fixed and that the *c* axis is aligned in a direction close to perpendicular to the long axis of the rod as would be described by Model A. This molecular weight range is also characterized by the fact that the morphological form is the same for all crystallization temperatures except when rapidly crystallized (quenched). This latter procedure yields well-developed type-(a) spherulites.

Selected values of the degree of crystallinity, as calculated from density and enthalpy of fusion measurements, are given in Table III for these molecular weights and morphology. Although a more extensive discussion of all the thermodynamic parameters obtained in this work will be given shortly we can note at this point that the samples in this grouping are highly crystalline. Furthermore, at these high levels of crystallinity there is a very good agreement between the degrees of crystallinity calculated by either method.[15]

Studies over the molecular weight range 8.08×10^4 to 2.49×10^6 constitute the major portion of this work. The results are much more complex than those previously described. At the higher crystallization temperatures the light scattering is azimuthally independent and is type (g) in our classification scheme. The morphology is thus rodlike with the breadth being a significant dimension. For the lower crystallization temperatures characteristic spherulitic patterns are observed which change from type (b) to (c) as the molecular weight is increased at a given crystallization temperature. The temperature, T_{sp}, at which the scattering pattern changes from spherulitic to nonspherulitic representation (b, c to g) is shown in more detail in Figure 7 as a function of molecular weight. These regions and their demarcation are also indicated in Figure 1. The value of T_{sp} initially rises with molecular weight and reaches an asymptotic value of 128–129 °C at $M_w = 2.52 \times 10^5$. For $M_w = 2.52 \times 10^5$ to 2.49×10^6, this temperature is essentially independent of molecular weight and the crystallization is isothermal. For the lower molecular weights, where T_{sp} is molecular weight dependent, the crystallization rate becomes very fast for crystallizations carried out below ~125 °C[9] and consequently may not be occurring isothermally. For $M_w \geq 252\,000$, $T_{sp} \simeq 128$ °C and consequently there can be no doubt that the crystallization is isothermal.

Typical SALS patterns both above and below T_{sp}, which allowed for the conclusions drawn above, and for the schematic of Figure 1 to be continued, are given in Figure 8 for $M_w < 10^6$ and Figure 9 for $M_w = 2.49 \times 10^6$ and 4×10^6. We shall consider first the result obtained for crystallization at temperatures above T_{sp}. For these samples, as has been stated above, the patterns are all circularly symmetric as is discerned in the figures. This type of pattern can theoretically arise from one of three different morphological forms. From Model A, circularly symmetric scattering would occur with rods when the optic axis is exactly aligned at an angle of either ~30 or ~70° to the long axis. Second, either Model A or Model B can

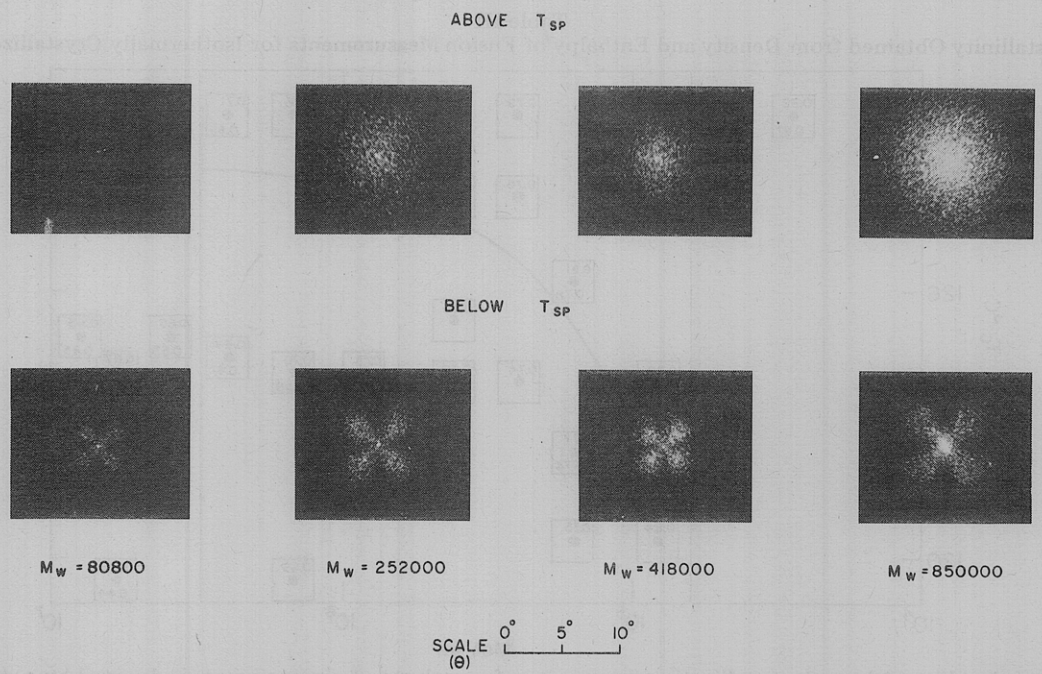

Figure 8. H_v small-angle light-scattering patterns for samples with $M_w = 8.08 \times 10^4$ to $M_\eta = 8.5 \times 10^5$ crystallized isothermally showing the two distinct patterns obtained above and below T_{sp}.

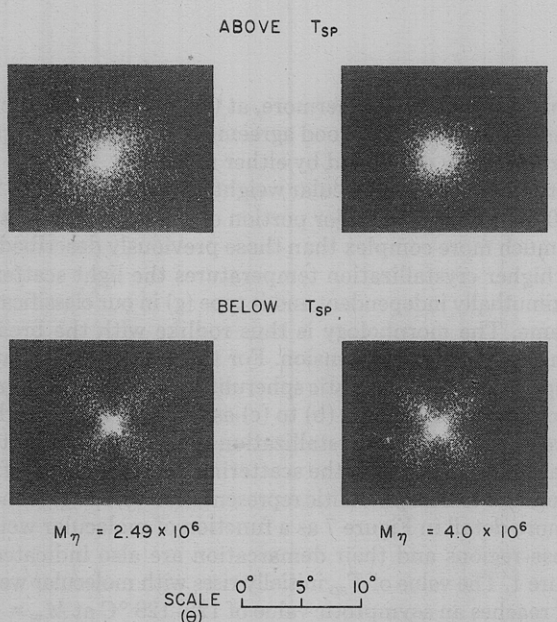

Figure 9. H_v small-angle light-scattering patterns for the fractions $M_\eta = 2.49 \times 10^6$ and $M_\eta = 4.0 \times 10^6$ crystallized isothermally above and below T_{sp}.

produce this pattern if the rods had finite width, and the width was comparable to the length. Lastly this type of scattering would also describe a system of randomly arranged lamellae. SALS cannot alone differentiate between these possibilities. To overcome this disadvantage light microscopy of these samples was also studied.

Typical light micrographs of these samples, illustrated in Figure 10, show structures which are not rodlike in the sense of those shown in Figure 6 for the lower molecular weights. They are generally symmetric in their dimensions with the size of the structures being of the order 10 μm. These structures are clearly different from those seen at lower molecular weights. The SALS patterns can now be reexamined with these results in mind. The possibility of random crystallites can be eliminated as a source of this scattering pattern, since the light micrographs show the presence of definite large structures. The only interpretation remaining is that the morphology is rodlike. Furthermore, the generally symmetric nature of the structures in the light micrographs strongly suggests an interpretation in terms of rods of finite width. The possibility of the symmetric patterns arising from rods with a precisely defined angle for the optic axis cannot be ruled out but would be a highly improbable event. The morphological interpretation of the data for these samples is therefore of structures whose rodlike characteristics are not as well defined as for the lower molecular weights.

The SALS patterns obtained below T_{sp} in Figure 8 are typical of a spherulitic morphology, which is well defined at the lower molecular weights in this region but whose structure and perfection progressively deteriorate as the molecular weight increases. In the region marked (c) in Figure 1 the SALS alone cannot distinguish between a poorly developed spherulite and a rodlike structure. A degradation of the spherulitic type (b) pattern is also observed for the higher molecular weight fractions with progressively lower crystallization temperature below 128 °C. In summary, although below T_{sp} a spherulitic structure predominates in this molecular weight range, the pattern is not as distinct as for the rapidly quenched samples and is indicative of poorly formed spherulites. The light micrographs confirm these conclusions. We note, therefore, that rapid crystallization results in the best developed internal macroscopic arrangement as embodied in spherulites.

The azimuthally independent SALS patterns observed here above T_s are due to large, but symmetric, structures as verified by light microscopy. An azimuthally independent SALS pattern is also observed for rapidly quenched samples of $M_\eta > 10^6$. However, in this case light microscopy reveals a total lack of organized structure. Thus, above T_{sp} in the molecular weight range under consideration a nonspherulitic, but organized, superstructure is formed which is similar in some respects to that observed at the lower molecular weights.

The sample of $M_\eta = 2.49 \times 10^6$, which represents the high end of this molecular weight grouping, is particularly interesting. We have already noted that when quenched this sample yields a pattern characteristic of randomly oriented crystallites. Results obtained for isothermal crystallization

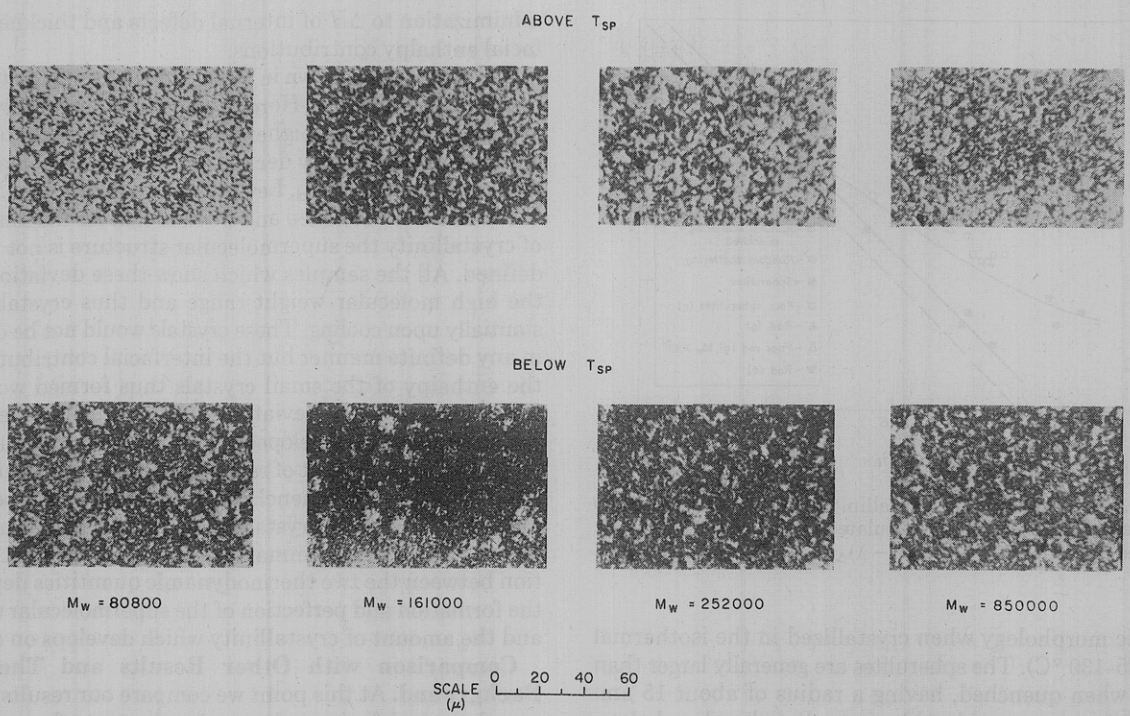

Figure 10. Polarized light micrographs from samples with $M_w = 8.08 \times 10^4$ to $M_\eta = 8.5 \times 10^5$ crystallized isothermally showing the two distinct morphologies above and below T_{sp}.

above and below T_{sp} for this molecular weight are given in Figure 9. Below T_{sp}, although azimuthally dependent the spherulitic nature of the pattern is very poor and might even be considered to be rodlike. However, above T_{sp}, an azimuthally independent pattern is definitely observed. Thus the major temperature dependent morphology, characteristic of the lower molecular weights, is observed. This behavior is also observed for the sample of $M_\eta = 4.0 \times 10^6$. These two samples are, therefore, unique in that three different scattering patterns, reflecting three different morphologies, can be observed depending on the crystallization conditions. The sample $M_\eta = 4 \times 10^6$ also is unique in that this sample behaves out of context if we classify our samples purely on the basis of viscosity average molecular weight. The SALS pattern for $M_\eta = 2.49 \times 10^6$ crystallized below T_{sp}, which we have designated as (c) in the schematic, is typical of the degradation of the type (b) pattern for the lower molecular weights. This pattern does not show any maximum at $\mu = 45°$ which is a characteristic of a well-defined spherulite. However, we have designated this as a type (c) pattern since the light micrographs are very similar to the type (b) designation typical of the lower molecular weights. It is also consistent with the previous work on mixtures.[8] Irrespective of the specifics of the classification there is a definite change in morphology at T_{sp}, as is observed for the other molecular weights in this grouping.

The thermodynamic quantities for these samples are given in Table III and will be discussed in detail subsequently in the context of the complete set of data that has been obtained. In examining the data, we should recollect[9,38] that in the high molecular weight end of this range (1.5, 2.5, and 4×10^6) there is considerable crystallization upon cooling subsequent to long-time isothermal crystallization at an elevated temperature.

In the last grouping of fractions, consisting of $M_\eta = 3$, 6, and 8×10^6, SALS patterns and light micrographs obtained for isothermal temperature crystallization are essentially the same as those observed in the rapidly crystallized material for the corresponding molecular weights.[57] Typical SALS patterns are shown in Figure 11. They are azimuthally independent and are interpreted as scattering from randomly arranged lamellae with no correlations in orientation. The light micrographs show no large structures present and are consistent with the SALS interpretation. At these molecular weights, therefore, no organized superstructure is formed under any crystallization conditions. This morphology is also indicated in Figure 1, and the thermodynamic data are listed in Table III.

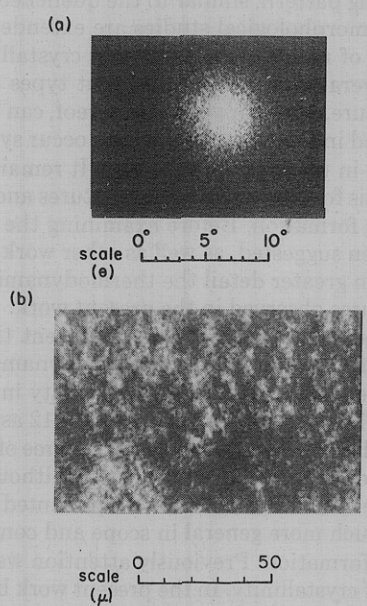

Figure 11. H_v small-angle light-scattering pattern and polarized light micrograph for the fraction $M_\eta = 6.09 \times 10^6$ crystallized isothermally at 119.5 °C.

To complete this aspect of the morphological studies the patterns resulting from the isothermal crystallization of the unfractionated parent polymers were also investigated. Marlex-50, the lowest molecular weight sample, shows a

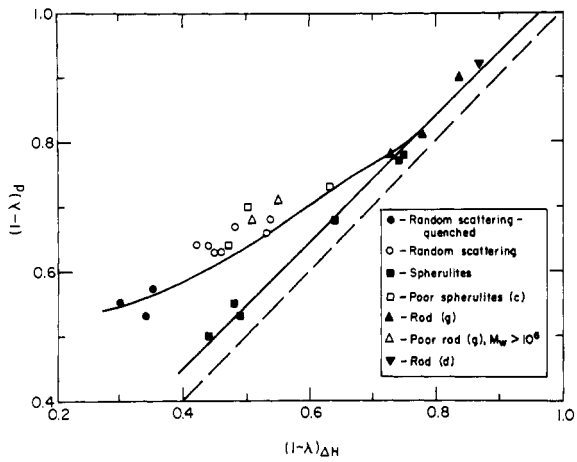

Figure 12. Plot of the level of crystallinity calculated from density against the level of crystallinity calculated from enthalpy of fusion. The dashed line is for $(1 - \lambda)_d = (1 - \lambda)_{\Delta H}$.

spherulitic morphology when crystallized in the isothermal region (125–130 °C). The spherulites are generally larger than observed when quenched, having a radius of about 15 μm. However, they are considerably more disordered and show considerable excess scattering. They would also be of the (b) type in the classification scheme. Both of the Hifax polymers, when crystallized at the higher temperatures, display a random scattering pattern, similar to the quenched case.

When the morphological studies are extended to include a wide range of molecular weights and crystallization temperatures several distinctively different types of supermolecular structure, or minor variants thereof, can be observed. As is indicated in Figure 1, the changes occur systematically with changes in these major variables. It remains to understand the basis for these different structures and the mechanism of their formation. Before examining the possibilities that have been suggested, as well as other work in this area, we examine in greater detail the thermodynamic properties of the structures observed in the present work.

Thermodynamic Quantities. To present these data in their most effective manner, the thermodynamic quantities were converted to the degree of crystallinity in the conventional way. The results are given in Figure 12 as a plot of degree of crystallinity from density against degree of crystallinity calculated from the enthalpy of fusion. Although this plot displays some of the features that were presented several years ago,[15] it is much more general in scope and contains a great deal more information. Previously attention was given only to the level of crystallinity. In the present work both the level of crystallinity and the supermolecular structure were varied. As can be seen from Table III and Figure 12, the degree of crystallinity on either basis does not lead to a unique supermolecular structure. This fact in turn affects the relationship between the two quantities.

There are essentially two groups of results indicated in Figure 12. In one set the plot falls very close to the straight line $(1 - \lambda)_d = (1 - \lambda)_{\Delta H}$, i.e., the degrees of crystallinity calculated by either method are very close to one another. The data delineated by the straight line in Figure 12 represent organized lamella systems which are well developed irrespective of whether the supermolecular structure is spherulitic or either of the two rod types observed. These data encompass a range of crystallinities from 0.5 to 0.9. They include these various type structures and do not depend on whether they are produced by quenching or long-time isothermal crystallization. We must then conclude that it is the organization of the lamella which lead to the concordance of the methods and a minimization to ΔH of internal defects and thickness/interfacial enthalpy contributions.

The other curve shown in Figure 12 is very similar to the one previously reported.[15] Here there is agreement between the two quantities at the higher levels of crystallinity but as the amount of crystallinity decreases $(1 - \lambda)_{\Delta H}$ becomes significantly less than $(1 - \lambda)_d$. Levels of crystallinity, on a ΔH basis, as low as 0.3 are obtained and we note that for the same degree of crystallinity the supermolecular structure is not uniquely defined. All the samples which show these deviations are in the high molecular weight range and thus crystallize substantially upon cooling. These crystals would not be organized in any definite manner but the interfacial contribution from the enthalpy of the small crystals thus formed would be a factor in causing the deviations. However, all of the samples either have poorly developed supermolecular structures, rods, or spherulites or consist of random scattering elements. In this latter category the quenched samples show a much larger deviation than those crystallized at an elevated temperature and then cooled. In summary, we can conclude that the relation between the two thermodynamic quantities depends on the formation and perfection of the supermolecular structure and the amount of crystallinity which develops on cooling.

Comparison with Other Results and Theoretical Background. At this point we compare our results with the morphological forms and growth rates recently reported by Hoffman et al.[10] A series of linear polyethylene fractions with molecular weights from 3.6×10^3 to 8.07×10^5 were studied by light microscopy. Although these results are in general broad agreement with those reported here, there are some discrepancies which involve the supermolecular structures formed and the molecular weights where changes in morphology occur. Only three distinct morphological forms were reported previously:[10] axialites, coarse-grained nonbanded spherulites, and irregular spherulites. Clearly the axialites are the same as our rod structures, type (d), and the coarse-grained nonbanded spherulites are identical with our disordered spherulites. We do not observe structures which we can directly identify with irregular spherulites. Our type (g) rodlike structures were not observed at all. Because of the restricted molecular weight range that was studied by Hoffman et al. they did not observe random crystallite structure.

For isothermal crystallization axialites were only observed[10] for $M_w = 3.6 \times 10^3$ to 1.8×10^4; for $M_w = 1.8 \times 10^4$ to $M_w \simeq 1.15 \times 10^5$ either axialites or spherulites were obtained depending on the crystallization temperature; for $M_w \simeq 1.15 \times 10^5$ to $M_w = 8.07 \times 10^5$ irregular spherulites were observed at all temperatures.

In addition to the new morphological forms that we have found there are two major discrepancies between these two works in the isothermal crystallization region. The first of these is that we observe rods, or axialites, for molecular weights up to 4.62×10^4, and for $M_w = 8.08 \times 10^4$ the temperature at which the change from rods to spherulites takes place is much less than that of Hoffman et al. The other is that we observe the two morphologies for molecular weights up to and including 2.49×10^6. With respect to the latter point we have already alluded to expected effects of polydispersity much of which has not as yet been investigated in detail. Hoffman et al.[10] have shown that the particular whole polymer that they studied was spherulitic at all crystallization temperatures and we have made similar observations for Marlex-50 which has a predominance of low molecular weight species. It seems reasonable to conclude, therefore, that the differences in the two works for M greater than 1.5×10^5 could lie in the polydispersity of the sample. In one case[10] only irregular spherulites are observed, while in the other there is a distinct change in the morphological form with crystallization temperature. This would appear to be confirmed by the rel-

atively large values, of 1.3 to 1.8, for M_w/M_n in the previous work.[10]

The explanation of the discrepancy in the lower molecular weight range, concerned primarily with the limits for the formation of rodlike structures, is not obvious. Polydispersity would not appear to be a major problem in this case since M_w/M_n is 1.1 or less for both sets of samples. In their sample preparation, Hoffman et al. filtered hot solutions of each fraction through millipore filters (0.2 μm). This process appears to remove many potential crystallization nuclei from the sample as larger size structures are observed. In our samples the structures observed are generally smaller. However, attempts to increase their size by using the same filtration technique proved to be unsuccessful. Furthermore, the use of this filtration method did not alter the morphological changes observed at the higher molecular weights. The effect of additives in reducing spherulite sizes is well known. However, other parameters such as the level of crystallinity from x ray and density remain unchanged, as do the x-ray diffraction line widths and positions.[44] It would seem likely that although we were unable to remove these nucleation centers (if present in our samples) they should have no effect on the supermolecular structure. We are unable, therefore, to explain this particular discrepancy between the two sets of data.

Despite these differences in the two works, they both display the same major features for isothermal crystallization for the same molecular weight range. At low molecular weights a rodlike morphology is observed at all temperatures; at intermediate molecular weights there is a crystallization temperature where the morphology changes from spherulitic to a different type rod (type g).[58] The major differences are the molecular weights at which these changes occur. For the much higher molecular weights, which were only studied here, the organized supermolecular structure is lost at all crystallization temperatures.

Hoffman and co-workers also studied the growth kinetics of the three morphological forms that they observed.[10] They found experimentally that the temperature coefficient of the axialites was twice that of the coarse-grained nonbanded spherulites. Since these results will undoubtedly play some role in the ultimate understanding of the mechanisms for the formation of all the supermolecular structures we briefly review the theory used to explain them.[49] The theory used is attributed to Lauritzen[49] which follows that of Sanchez and DiMarzio.[50] The latter[50] is essentially a modification to polymers of earlier work of Hillig[51] for low molecular weight substances. We may note parenthetically at this point that the polymer modified theory does not require any assumptions, directly or indirectly, with respect to the interfacial structure.

In his original analysis, Hillig[51] considers two extreme cases of crystal growth on a substrate. These have now been named regime I and regime II respectively when applied to polymers.[10] In the first case, regime I, the growth step is allowed to sweep completely across the face of the crystal and a pause occurs before the next layer is nucleated. In other words, the rate of lateral growth, g, of a nucleus across the face of the crystal is very much faster than the nucleation rate, i, per unit area of substrate. The net growth rate perpendicular to the crystal face, G, is thus proportional to i. More formally, the number of nuclei which form from time t to $t + dt$ on the surface of a crystal face, which nucleated itself at time $t = 0$, is given by

$$dn = \pi L^2 i \, dt \tag{7}$$

where L is the radius of the crystal face. If the rate of forming a growth layer is G/b where b is the thickness of a growth step, then the number of nuclei formed in time b/G must be equal to unity. Thus $n = 1$ when $t = b/G$

$$\int_0^{b/G} \pi L^2 i \, dt = 1 \tag{8a}$$

so that

$$G/b = \pi L^2 i \quad \text{or} \quad G = \pi b L^2 i \tag{8b}$$

For the other case, regime II, it is assumed that new growth steps are allowed to nucleate before the previous layer has filled the substrate. For these conditions the growth rate, G, will clearly be dependent on both g and i so that the number of nuclei formed in time t to $t + dt$ on the surface of a crystal face which nucleated at $t = 0$ is given by

$$dn = \pi (gt)^2 i \, dt \tag{9}$$

Under these conditions, the number of nuclei formed in time b/G can also be approximated by unity. However, in this case the initial nucleus has not grown to fill the entire substrate, thus

$$\int_0^{b/G} \pi (gt)^2 i \, dt \approx 1 \tag{10a}$$

and

$$G = (\pi/3)^{1/3} b g^{2/3} i^{1/3} \tag{10b}$$

Since the temperature coefficient of the growth rate will be dominated by the nucleation rate it is clear that they will be different in the two cases.

Sanchez and DiMarzio[50] have modified Hillig's work, adapting it to polymers, by reducing by one the dimensionality of the lateral growth along a crystal face. The length, l, of a nucleus or growth strip is assumed constant being only determined by the initial crystallization condition, that is the undercooling. The growth, G, in this formalism is controlled by the lateral dimension of the crystal face L, as well as the initiation and growth rates G and i. It is these three parameters which determine the undercooling at which the change in growth mechanism will occur.[49] Equations 3b and 10b can thus be simply transcribed to

$$G^{(I)} = lbLi \tag{11a}$$

$$G^{(II)} \approx l^{1/2} b (ig)^{1/2}/2 \tag{11b}$$

Since g will in general have a Boltzmann-type temperature dependence and i will have the usual nucleation dependence, the overall temperature dependence of $G^{(I)}$ and $G^{(II)}$ will be determined primarily by i. Hence in terms of nucleation theory $G^{(I)}$ and $G^{(II)}$ will be governed by the following approximate relation

$$\frac{d(\ln G^{(II)})}{d([T\Delta T]^{-1})} \Big/ \frac{d(\ln G^{(I)})}{d([T\Delta T]^{-1})} \approx 1/2 \tag{12}$$

Thus for the two extreme cases considered, the temperature coefficients of the growth rates differ by a factor of 2.

The case where the nucleation rate is much larger than the lateral growth rate g has also been considered.[52] This situation corresponds to the deposition of stable nuclei on the substrate with either minimal or no further lateral growth. Thus g can be ignored and the problem treated statistically.[52] It was then found for this case that[52]

$$G \sim i \tag{13}$$

which has exactly the same temperature dependence for the growth rate as has been found for the case designated as regime I, but this mechanism was not considered for this situation.[10]

Irrespective of the particular formulation chosen to represent the growth rate G there is no a priori or obvious reason for any of the mechanisms described, i.e., the relation between lateral growth and nucleation rate to lead to a particular

morphology or supermolecular structure. However, for the changes observed for rods or axialites as compared to spherulites some intuitive correlations can be made. In regime I, where a layer is rapidly filled by a single nucleation step, the propagation of lamella into rodlike structure could be expected, since there would be no other mode by which lamellae could grow. If, on the other hand, spherulites form as a consequence of the noncrystallographic branching of lamellae then the multiple nucleation of a layer could possibly lead to such a structure.

Unfortunately the development of supermolecular structures is not limited to these two simple morphologies. To explain the structures that have been observed so far, and in some cases their temperature coefficient of growth, the theoretical concepts just described must either be shown to be special cases of a more general theory or discarded. They appear to be the first steps in the direction of explanation.

For example, breaks in the growth rate are not limited to changes from axialites to spherulites,[6,53] nor is the ratio of the growth coefficients for the high- to low-temperature forms always two. In the case of polyoxymethylene[6] spherulites are formed at temperatures below the break and hedrites above. Although it is not clear whether the hedrites described are different from axialites or rods the ratio of the temperature coefficient of the hedrites to spherulites is now only one-half. For branched polyethylene,[53] on the other hand, spherulites are observed at temperatures above and below the break. Here the ratio of temperature coefficients is one-fourth, quite different from that for linear polyethylene and polyoxymethylene.

In our study of the supermolecular structure of linear polyethylene we have observed rather significant changes with molecular weight. The influence of molecular weight is not implicitly contained in the theory outlined, which again indicates its present restrictive nature. Of particular importance, in terms of experimental observation, as is indicated in the schematic outline of Figure 1, is the very high molecular weight region where random crystallites are formed at all crystallization temperatures. In so far as the temperature coefficients of overall crystallization rate and the growth rate can be compared some interesting observations can be made. The temperature coefficient for overall crystallization of high molecular weight at all temperatures and that for high temperatures of the lower molecular weights is twice that of the low temperature low molecular weights.[9] For the low molecular weights (≤ 1–2×10^6) this would correspond to the rod (axialite)-spherulite change. The same temperature coefficient for the rods (low molecular weight) and the random crystallites (high molecular weight) suggest that the growth rates are of the same functional form. This concept can be reconciled if the proposed growth mechanism of the rods follows this first case and the random crystallization the third case. There is in these results an interesting correlation with the Avrami exponent for overall crystallization at high temperatures as determined by dilatometry.[9] For $M_w = 7.8 \times 10^3$ to $M_w = 1.2 \times 10^6$, the value of the Avrami exponent n is 3, whereas for $M_w \geq 3 \times 10^6$, $n = 2$. Also the data for $M_w = 1.2 \times 10^6$ show the earliest deviation with degree of crystallinity of the Avrami theory for $n = 3$ and could be considered as transitional between $n = 3$ and 2. Although these Avrami exponents cannot be given a unique interpretation the change from $n = 3$ to 2 for a two-dimensional growth habit is indicative of an interfacial-controlled linear growth changing to diffusion-controlled growth. Alternatively the growth habit can be changing from two-dimensional to one-dimensional growth with the maintenance of the interface controlled linear growth. In either case the growth process is changing while the same temperature coefficient is maintained. It would thus seem very unlikely if the same case or regime were operative in both molecular weight ranges. A diffusion-controlled growth could be rationalized with the third case presented and would be consistent with the temperature coefficient of growth, the Avrami exponent, and the lack of formation of supermolecular structure. We have already noted[8] that when crystallized from diluent, so that diffusion-controlled growth is severely reduced or eliminated, these very high molecular weight samples develop organized supermolecular structures in the form of spherulites.

In summary we have observed a variety of morphological forms when an extended range of molecular weights and crystallization conditions were studied. These results are not directly explicable by the limited theoretical developments presently available.[10,49] However, the major features of these new observations can set the direction for further work along these lines. The extreme situations are as follows. At lower molecular weights, where high levels of crystallinity are developed under isothermal conditions, the growth is interface controlled and the growth faces are complete by just one nucleation act. Rodlike structures are then formed from the lamella crystallization. At the very high molecular weights the growth is diffusion controlled and consequently no supermolecular structures are observed. The best formed spherulites are formed under the most rapid crystallization conditions which for linear polyethylene corresponds to 115–120 °C.[54] This would yield a rapid nucleation rate, multiple nucleation acts on a given crystal face, and a strong propensity for noncrystallographic branching. The process should lead to spherulitic type structure. These extremes will have to be incorporated into a general theory from which the intermediate situation observed must follow. These differences in morphology are accompanied by major differences in thermodynamic quantities in some cases and very possibly in other properties as well.[55]

Acknowledgment. This work was supported by the National Science Foundation under Grant No. DMR 76-21925.

References and Notes

(1) L. Mandelkern, *J. Phys. Chem.*, **75**, 3909 (1971).
(2) L. Mandelkern, "Characterization of Materials in Research, Ceramics and Polymers", Syracuse University Press, Syracuse, N.Y., 1975, Chapter 13.
(3) L. Mandelkern, *Acc. Chem. Res.*, **9**, 81 (1976).
(4) P. H. Geil, "Polymer Single Crystals", Wiley-Interscience, New York, N.Y., 1963.
(5) A. Galeski and M. Kryszewski, *J. Polym. Sci.*, **12**, 471 (1974).
(6) Z. Pelzbauer and A. Galeski, *J. Polym. Sci., Part C*, **38**, 23 (1972).
(7) S. Go, R. Prud'homme, R. S. Stein, and L. Mandelkern, *J. Polym. Sci., Polym. Phys. Ed.*, **12**, 1185 (1974).
(8) L. Mandelkern, S. Go, D. Peiffer, and R. S. Stein, *J. Polym. Sci., Polym. Phys. Ed.*, **15**, 1189 (1977).
(9) E. Ergoz, J. G. Fatou, and L. Mandelkern, *Macromolecules*, **5**, 147 (1972).
(10) J. D. Hoffman, L. J. Frolen, G. S. Ross, and J. I. Lauritzen, Jr., *J. Res. Natl. Bur. Stand., Sect. A*, **79**, 671 (1975).
(11) J. G. Fatou and L. Mandelkern, *J. Phys. Chem.*, **69**, 71 (1965).
(12) R. Chiang, *J. Polym. Sci.*, **36**, 91 (1959).
(13) R. S. Stein, "New Methods of Polymer Characterization", B. Ke, Ed., Wiley-Interscience, New York, N.Y., 1964.
(14) R. Chiang and P. J. Flory, *J. Am. Chem. Soc.*, **83**, 2057 (1961).
(15) L. Mandelkern, A. L. Allou, Jr., and M. Gopalan, *J. Phys. Chem.*, **72**, 309 (1968).
(16) L. Mandelkern, J. G. Fatou, R. Denison, and J. Justin, *J. Polym. Sci.*, **3**, 803 (1965).
(17) R. S. Stein, "Structure and Properties of Polymer Films", R. W. Lenz and R. S. Stein, Ed., Plenum Press, New York, N.Y., 1972.
(18) R. S. Stein, A. Misra, T. Yuasa, and A. Wasiak, *Polym. Prepr., Am. Chem. Soc., Div. Polym. Chem.*, **16**, 13 (1975).
(19) A. Konda, K. Nose, and H. Ishikawa, *J. Polym. Sci., Polym. Phys. Ed.*, **14**, 1495 (1976).
(20) C. Picto, G. Weill, and H. Benoit, *J. Polym. Sci., Part C*, **16**, 3976 (1968).
(21) T. Pakula, M. Kryszewski, and Z. Soukup, *Eur. Polym. J.*, **12**, 41 (1976).
(22) F. Van Antwerpen and D. W. Van Krevelen, *J. Polym. Sci., Polym. Phys. Ed.*, **10**, 2423 (1972).

(23) R. E. Prud'homme, L. Bourland, R. T. Natarajan, and R. S. Stein, *J. Polym. Sci., Polym. Phys. Ed.*, **14**, 1541 (1976).
(24) R. E. Prud'homme and R. S. Stein, *Eur. Polym. J.*, **13**, 365 (1977).
(25) T. Hashimoto and R. S. Stein, *J. Polym. Sci., Part A-2*, **9**, 1747 (1971).
(26) R. S. Stein and W. Chu, *J. Polym. Sci., Part A-2*, **9**, 1137 (1970).
(27) T. Hashimoto, K. Nagatoshi, A. Todo, and H. Kawai, *Polymer*, **17**, 1075 (1976).
(28) T. Hashimoto, Y. Marakami, and H. Kawai, *J. Polym. Sci., Polym. Phys. Ed.*, **13**, 1613 (1975).
(29) M. B. Rhodes and R. S. Stein, *J. Polym. Sci., Part A-2*, **7**, 1539 (1969).
(30) J. J. van Aarten, *Eur. Polym. J.*, **6**, 1095 (1960).
(31) R. J. Samuels, *J. POLYM/ Sci., Part A-2*, **7**, 1197 (1969).
(32) E. P. Chang and J. S. C. W. Chien, *Macromolecules*, **5**, 610 (1972).
(33) G. L. Wilkes, *Mol. Cryst. Liq. Cryst.* **18**, 165 (1972).
(34) R. E. Prud'homme and R. S. Stein, *J. Polym. Sci.*, **12**, 1805 (1974).
(35) N. Hayashi and H. Kawai, *Polym. J.*, **3**, 140 (1972).
(36) M. Montani, N. Hayashi, A. Utsuo, and H. Kawai, *Polym. J.*, **2**, 74 (1971).
(37) Y. Murakami, N. Hayashi, T. Hashimoto, and H. Kawai, *Polym. J.*, **4**, 452 (1973).
(38) E. Ergoz, Ph.D. Dissertation, Florida State University, 1970.
(39) F. P. Price, *J. Polym. Sci.*, **37**, 71 (1959).
(40) D. Y. Yoon, C. Chang, and R. S. Stein, *J. Polym. Sci., Polym. Phys. Ed.*, **12**, 209 (1974).
(41) K. Sasaguri, S. Hoshino, and R. S. Stein, *J. Appl. Phys.*, **35**, 47 (1964).
(42) T. Oda, S. Nomura, and H. Kawai, *J. Polym. Sci.*, **3**, 1993 (1965).
(43) J. Dlugosz, G. V. Fraser, D. Grubb, A. Keller, J. A. Odell, and P. L. Goggin, *Polymer*, **17**, 471 (1976).
(44) A. G. M. Last, *J. Polym. Sci.*, **39**, 543 (1959).
(45) M. G. Broadhurst, *J. Res. Natl. Bur. Stand., Sect. A*, **70**, 481 (1966).
(46) P. J. Flory and A. Vrij, *J. Am. Chem. Soc.*, **85**, 3548 (1963)
(47) J. G. Fatou and L. Mandelkern, *J. Phys. Chem.*, **69**, 417 (1965).
(48) P. J. Flory, *J. Chem. Phys.*, **17**, 223 (1949).
(49) J. I. Lauritzen, Jr., *J. Appl. Phys.*, **44**, 4353 (1973).
(50) I. C. Sanchez and E. A. DiMarzio, *J. Res. Natl. Bur. Stand., Sect. A*, **76**, 213 (1972).
(51) W. B. Hillig, *Acta Metall.*, **14**, 1868 (1966).
(52) I. C. Sanchez and E. A. DiMarzio, *J. Chem. Phys.*, **55**, 893 (1971).
(53) T. Pakula and M. Kryzwski, *Eur. Polym. J.*, **12**, 47 (1976).
(54) L. Mandelkern, "Crystallization of Polymers", McGraw-Hill, New York, N.Y., 1964, p 228.
(55) R. A. Komoroski, J. Maxfield, F. Sakaguchi, and L. Mandelkern, *Macromolecules*, **10**, 550 (1977).
(56) The term randomly arranged lamellae is used throughout this work to describe a system of lamellae stacks where the correlations in orientation are random between individual stacks or domains.
(57) We have already noted that the fraction $M_\eta = 4 \times 10^6$ is anamolous in this group and displays morphological behavior of a slightly lower molecular weight.
(58) For theoretical reasons Hoffman et al.[10] calculated the undercooling at which the change from one morphological form to the other occurred and found it to be 17.5 ± 0.5 °C for all the molecular weights that are involved. Unfortunately they used a variant[45] of the theory of Flory and Vrij[46] for the melting of molecular crystals. The theory requires that all chains be of exactly the same length and hence cannot be applied to any real polymer system.[46,47] However, for very high molecular weights, such as 2.49×10^6, the melting temperatures for the different models are virtually indistinguishable from one another. For this molecular weight the transition from spherulites to (g) type rods occurs at 128 °C corresponding to an undercooling of 17.5–18 °C in agreement with the erroneous calculation. However, the correct results for the lower molecular weights needs to be recalculated using the theory for the equilibrium melting temperature of finite chains.[47,48] When this is done essentially a constant undercooling, within the limits of the calculation, is still found.

Spin-Label Study of the Poly(methacrylamide)-Type Copolymers in Solution

J. Labský, J. Pilař, and J. Kálal*

Institute of Macromolecular Chemistry, Czechoslovak Academy of Science, 162 06 Prague 6, Czechoslovakia. *Received April 14, 1977*

ABSTRACT: A series of soluble copolymers of *N*-(2-hydroxypropyl)methacrylamide with 4-nitrophenyl esters of ω-methacryloylamino acids were prepared. By a polymeranalogous reaction with 4-amino-2,2,6,6-tetramethylpiperidine-1-oxyl a spin-label was bonded to the copolymers at the ends of side chains of varying length. The mobility of spin-labels thus bonded was studied by the EPR method in methanol solution over the temperature range 213–313 K. The correlation time τ, characterizing the mobility of the spin-label, depends monotonically on the length of the side chain; at 293 K, τ of the copolymers under investigation varies from 1×10^{-10} to 1×10^{-9} s as the number of methylene groups in the amino acid rises from 0 to 11. The activation energy of these motions, E_{act} = 3 kcal/mol, remains the same for all copolymers.

(I) Introduction

The design of water-soluble synthetic polymers as carriers of biologically active groups[1] and enzymatically cleavable bonds[2] needs information about the behavior of various side chains in solution. Therefore effective experimental approaches to conformation and mobility studies of side chains of soluble polymers are needed, one of which is EPR spin labeling. It is well known that the shape of the EPR spectra of nitroxides in solutions depends on the rotational motion (characterized by the correlation time) of the nitroxide group relative to the applied magnetic field, owing to the anisotropy of the hyperfine interaction tensor of the unpaired electron with the nucleus of the nitrogen atom and to the anisotropy of their *g* factor.[3] The rotational motion of the nitroxide group is influenced by the medium, which motivates the use of the above properties in an investigation of the properties of the medium. Nitroxide can be either only physically dispersed in the medium as a spin probe or be chemically bonded as a spin label. An example of the use of spin labels in the study of the motions of polymer segments is a paper by Bullock, Cameron, and Smith.[4] Here we report a study of the mobility of spin labels bonded at the ends of variously long side chains of copolymers of the poly(methycrylamide) type in methanolic solutions.

(II) Experimental Section

Preparation of Copolymers. A series of copolymers of *N*-(2-hydroxypropyl)methacrylamide (HPMA) with 4-nitrophenyl esters of methacryloylated ω-amino acids was prepared. The monomers used are described in Table I. A general procedure for the preparation of these monomers and the preparation of copolymers with HPMA by precipitation copolymerization in acetone has been described earlier.[2,5,6] The copolymers were prepared so as to contain 3 mol % of the 4-nitrophenyl ester. Spectroscopic measurements[2] confirm that the concentration of the active ester in the copolymers does not differ from this value by more than 10%. The molecular weight of the copolymers was ca. 40 000. The numbers 2–15 used as subscripts in denoting the monomers indicate the lengths of their side chains.